

**This is the final draft of the contribution published as:**

**Laube, G., Schmidt, C., Fleckenstein, J.H. (2018):**

The systematic effect of streambed conductivity heterogeneity on hyporheic flux and residence time

*Adv. Water Resour.* **122**, 60 - 69

**The publisher's version is available at:**

<http://dx.doi.org/10.1016/j.advwatres.2018.10.003>

# The Systematic Effect of Streambed Conductivity Heterogeneity on Hyporheic Flux and Residence Time

Gerrit Laube; Christian Schmidt; Jan H. Fleckenstein

*Department Hydrogeology, Helmholtz Centre for Environmental Research – UFZ,  
Permoserstraße 15, 04318 Leipzig, Germany*

---

## Abstract

A systematic understanding of hyporheic flux (HF) and residence times (RT) is important as they are a major control of biogeochemical processing in streambeds. Previous studies addressing the effect of heterogeneity in streambed hydraulic conductivity (K) on HF and RT have come to deviating conclusions depending on the specific study design and the selection of heterogeneity cases being investigated. To more systematically evaluate the effects of conductivity heterogeneity on HF and RT, we simulated hyporheic exchange induced by idealized streambed ripples over a large range of heterogeneities. Conductivity heterogeneity was represented in the simulations in terms of 10,000 different heterogeneity realizations from a geostatistical model based on continuous Gaussian and discrete indicator random fields. We demonstrate that any isotropic homogeneous K-field, as an average of a heterogeneous K-field, can only match RT or HF of the respective heterogeneous K-field, but never both. We found exponential correlations of RT and HF with the variance of heterogeneous conductivity. Based on these correlations, an equivalent anisotropic homogeneous conductivity tensor  $K$  can be derived. This equivalent anisotropic  $K$  efficiently accounts for the effects of small scale heterogeneity on HF and RT. It can be calculated from the median and variance of the hydraulic conductivity distribution of the targeted heterogeneous sediment, without explicitly characterizing the sediment texture.

*Keywords:* conductivity heterogeneity, hyporheic exchange, residence time

---

## 1. Introduction

River networks play an important role in the processing of nutrients and pollutants (Seitzinger et al., 2006; Battin et al., 2008). Advective transport of solutes into the riverbed fuels this biogeochemical processing (e.g. Triska et al., 1989; Newcomer et al., 2018). Such advective transport is facilitated where pressure variations at the surface water-sediment interface occur (Elliott and Brooks, 1997). The bedform induced flow of surface water through the sediments is called hyporheic exchange and the zone the surface water flows through the

hyporheic zone (HZ) which fundamentally controls stream ecosystem functions  
10 such as the processing of solutes (see for example Boano et al. (2014) and refer-  
ences therein). Bedform-driven hyporheic exchange occurs along a contin-  
uum of scales of geomorphic features ranging from mm to dm sized ripples,  
dunes (dm to m), pool-riffle-structures (m to tens of m) and across meanders  
(tens to hundreds of m) (Boano et al., 2014). The spatial scale of features con-  
15 trols flow path lengths, the volume of the hyporheic zone and the residence  
time in the hyporheic zone (Stonedahl et al., 2013). Existing studies on ef-  
fects of morphology on hyporheic exchange have either focused on understand-  
ing the effects of individual features (e.g. Cardenas et al., 2008; Hester et al.,  
2013; Trauth et al., 2013) or the combined effects of multiscale morphological  
20 structures (e.g. Wörman et al., 2006; Stonedahl et al., 2010; Morén et al., 2017;  
Azizian et al., 2017). Many studies that analyze hyporheic exchange have as-  
sumed homogeneous sediments either for simplicity or to isolate the effects of  
morphology and hydraulic conditions from effects of sediment heterogeneity.  
The hydraulic properties of the sediment however, exert a strong control on hy-  
25 porheic exchange. Hydraulic conductivity(K) can vary over orders of magnitude  
and in turn controls the magnitude of hyporheic exchange flux (HF). Natural  
sediments are practically never homogeneous. Heterogeneity has been shown  
to affect HF and hyporheic RT (Cardenas et al., 2004; Salehin et al., 2004;  
Sawyer and Cardenas, 2009; Bardini et al., 2013; Hester et al., 2013; Gomez-Velez et al.,  
30 2014; Zhou et al., 2013; Pryshlak et al., 2015; Tonina et al., 2016; Liu and Chui,  
2017) and the geometry of hyporheic flowpaths (Cardenas et al., 2004; Salehin et al.,  
2004; Sawyer and Cardenas, 2009; Bardini et al., 2013; Fox et al., 2016). Un-  
derstanding how heterogeneity affects HF, RT or both is particularly important  
because a full characterization of sediment heterogeneity is hardly possible, espe-  
35 cially in complex field settings. Thus accounting for the effects of heterogeneity  
can help to reduce uncertainties in quantifying HF and RT arising from the  
assumption of homogeneity.

Previous studies, which have analyzed the effects of heterogeneity mostly  
reported increased HF and decreased RT with increasing heterogeneity, which  
40 translates into an increased homogeneous equivalent K (Cardenas et al., 2004;  
Salehin et al., 2004; Sawyer and Cardenas, 2009; Bardini et al., 2013; Hester et al.,  
2013; Zhou et al., 2013; Pryshlak et al., 2015; Fox et al., 2016; Liu and Chui,  
2017). This general observation was independent of the underlying heterogene-  
ity representation used in the studies, whether discrete or continuous, random  
45 or stratified. The magnitude of the reported effect varied from dominant (e.g.  
Zhou et al., 2013) to negligible (e.g. Salehin et al., 2004). In a few cases also  
opposing effects have been reported with heterogeneity causing a decrease in HF  
and an increase in RT (e.g. HF and median RT in Tonina et al. (2016) and the  
weakly heterogeneous "Massilon" case in Sawyer and Cardenas (2009)). Dif-  
50 ferent from other studies with randomized heterogeneity, Sawyer and Cardenas  
(2009) looked at one specific case of heterogeneity based on an outcrop anal-  
og with a low  $\log(K)$  variance ("Massilon":  $\sigma_{\ln K}^2 = 0.148$ ) and a thoughtfully  
placed dependence between bedform morphology and depositional structures.  
Tonina et al. (2016) used different realizations of one multigaussian heterogene-

55 ity model, but did not systematically evaluate other non-gaussian heterogeneity models. This highlights the importance of evaluating a larger variety of different heterogeneity types as well as different realizations to also account for potential anomalies in the results.

60 The assessment of effects of heterogeneity potentially also depends on the choice of an appropriate homogeneous reference case, which the heterogeneous case can be compared to (e.g Sawyer and Cardenas, 2009; Pryshlak et al., 2015). It is commonly taken from an equivalent homogeneous representation of hydraulic conductivity, which aims to reflect the effective conductivity of the heterogeneous domain. Simple statistical averages such as the arithmetic, geo-  
65 metric, or harmonic mean, or variants of these statistical measures have been applied to estimate an effective hydraulic conductivity based on stochastic flow theory (e.g. Zhang et al., 2006; Salehin et al., 2004). To account for structural anisotropy, an anisotropic equivalent  $K$  has been used (Durlofsky, 1991; Salehin et al., 2004; Sawyer and Cardenas, 2009). However, the true equivalent  
70 hydraulic conductivity can be quite different from those statistical measures particularly for strongly heterogeneous, structured conductivity fields (e.g. Fleckenstein and Fogg, 2008). Furthermore, equivalent hydraulic conductivities derived on the basis of heads and bulk flow may be quite different from those derived based on transport characteristics such as water residence times or solute  
75 arrival times (Scheibe and Yabusaki, 1998; Knudby and Carrera, 2005).

In homogeneous media, mass continuity requires that bedform driven hyporheic flux and mean RT are inversely proportional as long as the shape of the morphological features does not change (Elliott and Brooks, 1997). Higher hydraulic conductivity generally promotes higher HF and shorter RT. In hetero-  
80 geneous sediments, however, hyporheic zone volume and the geometry of flow paths can vary significantly with sediment structure, which differently affects RT and HF and hence the relationship between the two. Finding an equivalent homogeneous case based on statistics of the heterogeneity field, which adequately accounts for heterogeneity effects on both HF and RT would therefore be helpful  
85 for an improved evaluation of HF and RT in complex field settings. This paper contributes to this effort.

Streambed heterogeneity has been characterized using different techniques ranging from deterministic representations based on detailed field assessments (Chen, 2000; Genereux et al., 2008) or outcrop analogs (Sawyer and Cardenas,  
90 2009), over geophysical techniques (Crook et al., 2008; McLachlan et al., 2017) to geostatistical representations using smoothly or more discretely varying continuous or indicator random fields (Fleckenstein et al., 2006; Irvine et al., 2012; Hester et al., 2013; Tonina et al., 2016) or more complex geostatistical models that account for explicit structural elements in the sediments (Zhou et al.,  
95 2013).

All of these methods have their specific merits, but given the vast range of different field conditions, it is beyond the scope of this paper, to evaluate which ones are best suited to represent a specific type of streambed. Geostatistical simulations are generally well suited to systematically evaluate sediment  
100 heterogeneities in a Monte Carlo framework as they allow to create multiple

realizations of heterogeneity as well as different types. This approach is chosen here as we want to systematically evaluate the combined effects of sediment heterogeneity on HF and RT.

We focus on streambed dunes as these smaller morphological features are the most relevant for total hyporheic exchange (Stonedahl et al., 2013; Pryshlak et al., 2015). Bedform-driven hyporheic exchange with stochastically generated hydraulic conductivity fields is numerically simulated. The model setup is intentionally kept simple (2D domain, idealized bedforms and pressure variations at the streambed surface) in order to allow for a large number of scenarios and comparability to analytical solutions, which is in line with other systematic investigations on hyporheic exchange and residence times (Cardenas and Wilson, 2006; Boano et al., 2009; Hester et al., 2013; Tonina et al., 2016). In total 10,000 different geostatistical realizations of heterogeneous K fields were simulated with a 2D model setup representing a segment of a streambed with ripple-induced pressure variations at the sediment water interface. An analytical solution of hyporheic exchange fluxes and hyporheic residence time is derived for an anisotropic homogeneous sediment. In this way the effects of heterogeneity on HF and RT can be evaluated against a set of homogeneous reference cases. Statistical analysis of these effects and systematic evaluation of the closed-form solution of anisotropy allow for the development of an equivalent anisotropic K tensor. We show an equivalent K tensor that is estimated from statistical moments without specific knowledge of the heterogeneous texture and imitates its heterogeneous target with respect to HF and median RT.

## 2. Methods

### 2.1. Representation of Heterogeneous Sediments

The streambed conductivity heterogeneity is represented by multiple realizations of different types of random fields and their transformations, all based on sequential Gaussian simulations (SGSIM). All fields were calculated by the Stanford Geostatistical Modeling Software (SGeMS, Remy et al. (2011)). The five methods differ in the variogram model (Exponential, Gaussian, Spherical) and in the distribution transformation applied to it (Binary, Log-Normal, Zinn-Harvey). More specifically, the combinations *Gaussian* - Log-Normal, *Exponential* - Log-Normal, *Spherical* - Log-Normal, *Gaussian* - *Binary* and *Gaussian* - *Zinn-Harvey* were used as shown in Figure 1. The distribution transformations aim to change the conductivity distribution of the random fields from Gaussian, as provided by SGSIM, to a specified distribution, while preserving the original spatial correlation and visual appearance.

The *Binary* transformation assigns a predefined high or low conductivity value to the cells using their median as threshold. This creates a representation of two discrete hydrofacies with independent deposits and thus non-continuous K distributions. Such independent hydrofacies can be formed by channel and bedform migration (Lunt et al., 2004).

The *Log-Normal* transformation is commonly known as score transformation (Knudby and Carrera, 2005) or histogram transformation (Remy et al., 2011)

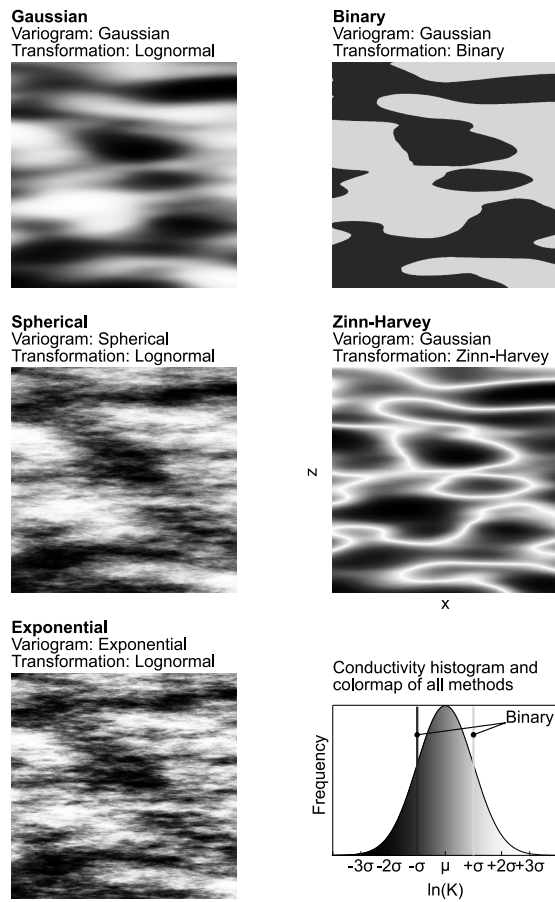


Figure 1: The five different random field methods used in this study, generated with the same input parameters and seeds to highlight differences in the methods. All methods but the binary have a log-normal distribution of conductivities.

145 targeting a log-normal distribution. More specifically, the cells are ranked by  
their conductivity values. Based on these ranks, corresponding conductivity val-  
ues are calculated from the quantile function of a log-normal distribution. This  
transformation ensures that all fields adhere to the same statistical distribu-  
tion (figure 1 lower right panel), a prerequisite for comparison between different  
150 fields.

The *Zinn-Harvey* transformation, also known as absolute-value transfor-  
mation, was developed by Zinn and Harvey (2003) and successfully used by  
Knudby and Carrera (2005) in order to obtain a better connected random field  
than the regular Gaussian random field. It was based on the idea that Gaussian  
155 random fields usually consist of poorly connected high/low conductivity areas  
embedded in a highly connected medium value matrix. Consequently, Zinn and  
Harvey developed a transformation that turns medium values into high values.  
More technically, the negative absolute values are taken from a normally dis-  
tributed Gaussian random field, hence turning high values to low values. This  
160 transform shifts the values, which had previously been in the medium range to  
higher values at the upper end of the new distribution. A *Log-Normal* trans-  
formation transforms this distribution to the targeted log-normal distribution  
of conductivity values. See (Knudby and Carrera, 2005) Figure 5 for an illus-  
tration of the method. The resulting fields have enhanced high-K connectiv-  
165 ity, which is common in many natural geologic media, e.g. alluvial sediments  
(Zheng and Gorelick, 2003).

The random fields are parametrized by the mean ( $\mu_{\ln K}$ ) of the natural loga-  
rithm of the hydraulic conductivity ( $K$ ), its standard deviation ( $\sigma_{\ln K}^2$ ), the two  
correlation lengths ( $lx$ ,  $ly$ ), i.e. the ranges of the underlying variograms and  
170 the azimuth of the variogram ( $\alpha$ ), which allows the creation of cross-bedding  
structures. Note, that some of the aforementioned transformations alter the  
correlation lengths of the random fields (Gong et al., 2013; Zinn and Harvey,  
2003). Therefore,  $lx$  and  $ly$  can not directly be compared between different  
transformations but only between fields transformed with the same method.

175 For each of the five random field methods, 2000 realizations were created,  
each with an individual randomized set of  $\sigma_{\ln K}^2$ ,  $lx$ ,  $ly$  and  $\alpha$  which sums up to  
the total of 10000 different heterogeneity fields being modeled. The parameter  
ranges were selected to cover the range of values reported in the literature.  $\mu_{\ln K}$   
was kept constant in all realizations at -8.9548.  $\sigma_{\ln K}^2$  was sampled from  $0 <$   
180  $\sigma_{\ln K}^2 < 6.76$  according to the values provided by  $\sigma_{\ln K}^2 = 0.148$  and  $\sigma_{\ln K}^2 = 0.937$   
(Sawyer and Cardenas, 2009; Bardini et al., 2013),  $\sigma_{\ln K}^2 = 1.0$  and  $\sigma_{\ln K}^2 = 2.0$   
(Salehin et al., 2004) up to  $\sigma_{\ln K}^2 = 6.65$  (Zhou et al., 2013). The case with  
the highest  $\sigma_{\ln K}^2 = 6.76$  corresponds roughly to a binary composition of silty  
loam ( $K \approx 10^{-5}$  m/s) and medium to coarse gravel ( $K \approx 1.7 \cdot 10^{-3}$  m/s). Gelhar  
185 (1993) reported  $0.24 < \sigma_{\ln K}^2 < 4.6$  to be commonly found in glacial groundwater  
bodies formed by fluvial or alluvial processes. The intervals of the remaining  
randomized parameters can be found in Table S1 in the supporting information.

## 2.2. Hydraulic Model

The subsurface model was set up as a 2D rectangular grid and discretized  
 190 into 2001 x 501 cells in horizontal and vertical direction, respectively. A sinu-  
 soidal hydraulic head distribution was applied at the sediment-water interface  
 representing a rippled riverbed (Figure 2). The fully saturated steady state flow  
 field within the domain was calculated using the finite volume model MIN3P  
 (Mayer et al., 2002).

195 The hydraulic head distribution at the interface and at the up- and down-  
 stream boundary is calculated as

$$h|_{z=0} = 0.28 \frac{U^2}{2g} \left( \frac{H}{0.34d} \right)^{\frac{3}{8}} \sin \left( \frac{2\pi}{\lambda} x \right) - sx \quad (1)$$

according to Elliott and Brooks (1997), where U is the stream velocity, g is the  
 gravity, H is the bedform height, d is the stream depth,  $\lambda$  is the length of a  
 200 virtual bedform, s is the slope and x is the coordinate in flow direction, starting  
 at the upstream boundary of the domain. Equation 1 was originally developed  
 from experimental data of dunes ( $\lambda = 3ft$ , Fehlman, 1985)) but has since then  
 successfully been used to model also head distributions of shorter wavelengths  
 (e.g.  $\lambda = 15cm$ , Fox et al., 2014). In order to minimize effects of the upstream  
 205 and downstream boundaries, the head distribution of P=10 bedforms was ap-  
 plied to the domain of 2 m length and 0.5 m depth. All other hydraulic and  
 geometric parameters representing the stream and the bedforms were selected  
 based upon the “Massillon”-case from Sawyer and Cardenas (2009) and can be  
 found in Table S2 in the supporting information. As restrictions to the depth  
 210 of the streambed were not part of this study, an infinite depth domain was de-  
 sirable. Such an infinite domain depth was used in the analytical solution (Sec  
 2.3). The simulation domain, however, needs a bottom boundary. We chose a  
 no flow boundary at a depth of 0.5 m, which we tested to be sufficiently deep to  
 avoid boundary effects.

215 All random field realizations were simulated using the same model setup.  
 For further information on the parameterization see the source code and MIN3P  
 input file template in the supporting information.

## 2.3. Analytical Solution for Anisotropic Homogeneous Conductivity

The effects of heterogeneity are evaluated with respect to both isotropic  
 220 and anisotropic homogeneous sediments. In order to effectively generate the  
 homogeneous reference cases, an analytical solution is developed to solve the flow  
 field for an anisotropic homogeneous case. Isotropic homogeneity is a special  
 case of this general anisotropic solution. The residence time and hyporheic  
 flux are derived using the method of Elliott and Brooks (1997) as shown in  
 225 Appendix A. The most simple case of anisotropy with a diagonal conductivity  
 tensor

$$\mathbf{K} = \begin{bmatrix} K_{xx} & 0 \\ 0 & K_{zz} \end{bmatrix} \quad (2)$$

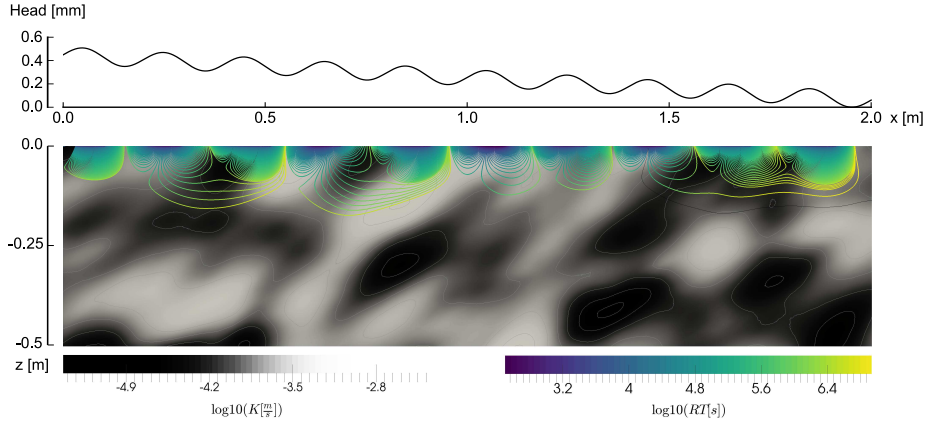


Figure 2: Simulated domain with a heterogeneous conductivity (red-white-blue) realization of the *Gaussian* method. Streamtraces were analyzed for their hyporheic residence time (rainbow). A sloping sinusoidal head boundary was applied at the top, which represents a rippled streambed.

and an anisotropy ratio of

$$r = \frac{K_{xx}}{K_{zz}} \quad (3)$$

230 is used to compare homogeneous anisotropic, homogeneous isotropic ( $r = 1$ ) and heterogeneous sediments.

It is shown in equation A.3 that for a semi-infinite domain without slope, the head field

$$h(x, z) = h_0 e^{\sqrt{r} \frac{2\pi}{\lambda} z} \sin\left(\frac{2\pi}{\lambda} x\right) \quad (4)$$

235 develops with the maximum boundary head amplitude  $h_0$ . It can be seen, that anisotropy affects the vertical expansion of the hyporheic zone, i.e. a lower vertical conductivity leads to a shallower hyporheic zone.

From this head field, the seepage velocity  $u_z$  of a hyporheic streamtrace infiltrating the sediment at point  $(x_0, z_0 = 0)$  is derived in equation A.12 as

$$240 \quad u_z(x_0) = -h_0 \frac{2\pi}{\lambda} \frac{K_{xx}}{\sqrt{r}} \sin\left(\frac{2\pi}{\lambda} x_0\right). \quad (5)$$

The magnitude of the volumetric flow is inversely proportional to the square root of the anisotropy ratio  $\sqrt{r}$ .

The exfiltration time  $t_e$  of a single particle infiltrating the sediment at  $x_0, z_0 = 0$  is derived in A.11 as

$$245 \quad t_e(x_0) = \frac{\Phi \lambda}{K_{xx} h_0 \pi} \frac{x_0}{\cos\left(\frac{2\pi}{\lambda} x_0\right)} \quad (6)$$

with the porosity  $\Phi$ .  $t_e$  is independent from  $r$ , which allows for the choice of arbitrary  $u_z$  to  $t_e$  ratios through changes in  $r$ . The calculation of anisotropic  $Q_H$

and flux-weighted  $\tilde{RT}$  from equation 5 and 6 yields rather complex equations without generating any more insight towards the general behavior of anisotropic hyporheic flux and residence time that could not be derived from equation 5 and 6.

For a mutual validation of both the analytical solution and the numerical simulations, selected homogeneous cases were calculated and simulated to test for equal behavior with respect to changes in  $K_{xx}$  and  $K_{zz}$ , by calculating and simulating three homogeneous cases with  $\ln K = [-8.95, -8.95]$ ,  $\ln K = [-8.95, -10.95]$  and  $\ln K = [-10.95, -10.95]$  to check for equal behavior with regard to changes in overall conductivity and anisotropy.

#### 2.4. Post-processing

Hyporheic residence times were evaluated using stream traces, calculated from the steady state flow field using ParaView (Ayachit and Avila, 2015). Seeds of the stream traces were placed in the cell centers of the uppermost layer. In the analysis were considered only those stream traces that both enter and exit the domain via the sediment-water interface, hence ignoring flow over the up- and downstream boundaries of the domain. Hyporheic fluxes were calculated from the seepage velocity at the infiltration points of the hyporheic stream traces.

The flux weighted median of the travel times of the stream traces ( $\tilde{RT}$ ) and the total hyporheic volumetric flow rate ( $Q_H$ ) were used as dependent variables to evaluate the influence of heterogeneity on hyporheic exchange. Additionally, to evaluate the heterogeneity-induced variations of hyporheic flowpaths, the *equivalent Volume* ( $V_{eq}$ ) was calculated from  $\tilde{RT}$  and  $Q_H$ . The underlying idea of  $V_{eq}$  is based on the fact that volume conservation requires

$$V = QRT \quad (7)$$

for an arbitrary streamtube, where  $V$  is the volume enclosed by the tube,  $Q$  is the volumetric flow rate and  $RT$  is the residence time. Similarly, the equivalent volume is calculated as

$$V_{eq} = Q_H \tilde{RT}. \quad (8)$$

If the flowpath geometries were invariant between different realizations,  $Q_H$  and  $\tilde{RT}$  would be related inversely proportional and thus  $V_{eq}$  stayed constant. In contrast, if a constant volumetric flow was focused on a decreasing volume fraction of the domain, the  $RT$  distribution (and thus  $\tilde{RT}$ ) shifted towards shorter residence times, independent from  $Q_H$ . Consequently,  $V_{eq}$  decreased.

In studies that have targeted aquifer heterogeneity in the context of stream-aquifer exchange, the importance of the uppermost sediment layer (represented by the top layer of the modeling domain) has been emphasized (Kalbus et al., 2009). Similarly for hyporheic exchange, hydraulic conductivities in the uppermost sediment layers are most decisive for net hyporheic flux ( $Q_H$ ) and median

residence time ( $\tilde{RT}$ ) as head gradients ( $|\nabla h|$ ) are largest there and decline exponentially with depth  $z$  according to equation 4

$$|\nabla h| = \sqrt{\left(\frac{\partial h}{\partial x}\right)^2 + \left(\frac{\partial h}{\partial z}\right)^2} \quad (9a)$$

$$|\nabla h| = h_0 \frac{2\pi}{\lambda} e^{\sqrt{r} \frac{2\pi}{\lambda} z} [\cos^2\left(\frac{2\pi}{\lambda} x\right) + \sqrt{r} \sin^2\left(\frac{2\pi}{\lambda} x\right)]. \quad (9b)$$

To evaluate this effect, the conductivity parameters  $\mu_{n,\ln K}$  and  $\sigma_{n,\ln K}$  were additionally calculated for the upper layer of  $\{1, 2, 4, 6, 8, 10, 20, 40, 100, 400\}$  mm thickness measured from the interface. For scale independent comparability, those sections of the uppermost layers were named by fractions of the bedform wavelength  $\lambda$ , i.e.  $n = \{0.5, 1, 2, 3, 4, 5, 10, 20, 50, 100, 200\}\% \lambda$ . Those upper-layer statistics have merely been recorded in post-processing, not modified in pre-processing, because the large variety of random fields provided sufficient variations in these upper-layer statistics.

With the additional upper layer statistics, the influence of a total of 29 different predictor variables, namely  $\mu_{n=0.5\dots 200\%}$ ,  $\sigma_{n=0.5\dots 200\%}$ ,  $\mu_{\ln K}$ ,  $\sigma_{\ln K}$ ,  $\sigma_{\ln K}^2$ ,  $\alpha$ ,  $l_x$ ,  $l_y$  and *randomfield method* on the three response variables  $\tilde{RT}$ ,  $Q_H$  and  $V_{eq}$  can be evaluated. In order to sort those predictors by their relative importance, a forward stepwise regression model was used (James et al., 2013). Such a model starts with a linear regression without any predictors and then, one at a time, adds the predictor that improves the model most. This method ultimately yields 30 linear regressions per response variable based on 0, 1, 2, ... 29 predictors. By the nature of this method, each additional predictor improves the fit to the training data set but not necessarily to an unseen validation data set. This leads to an overfit of the training data with additional predictor variables that are irrelevant when used with an unseen data set. This raises the need for an evaluation of the regressions on a test data set. We performed such an evaluation via cross-validation, which divides the data set in several combinations of training and test sets and calculates the actual improvement of the regressions on unseen data, allowing the selection of the most important predictors and omitting the less important ones.

### 3. Results

Streambed heterogeneity generally increased  $Q_H$  and decreased  $\tilde{RT}$  compared to an isotropic homogeneous streambed of equal  $\mu_{\ln K}$ . We found a decaying exponential relationship between  $\tilde{RT}$  and  $\sigma_{\ln K}^2$  and a positive exponential correlation between  $Q_H$  and  $\sigma_{\ln K}^2$ . A linear regression between  $\ln \tilde{RT}$  and  $\ln Q_H$  with  $\sigma_{\ln K}^2$  yielded

$$\tilde{RT}_{Het} = \begin{cases} e^{-0.89\sigma_{\ln K}^2} \tilde{RT}_{Hom}; R^2 = 0.75; & \text{for log-normal distributed K} \\ e^{-0.47\sigma_{\ln K}^2} \tilde{RT}_{Hom}; R^2 = 0.89; & \text{for binary distributed K} \end{cases} \quad (10)$$

325 and

$$Q_{H,Het} = \begin{cases} e^{0.36\sigma_{\ln K}^2} Q_{H,Hom}; R^2 = 0.67; & \text{for log-normal distributed K} \\ e^{0.24\sigma_{\ln K}^2} Q_{H,Hom}; R^2 = 0.79; & \text{for binary distributed K} \end{cases} \quad (11)$$

which results in the linear dependencies shown in in log-linear space in Figure 3 A and B. The coefficients of determination ( $R^2$ ) in equation 10 and 11 were calculated from logarithmic data as shown in Figure 3.

330 We found a decreasing relationship between  $V_{eq}$  and  $\sigma_{\ln K}^2$  (Figure 3 C), which indicates changes in the geometry of flowpaths between different scenarios. More specifically, in sediments characterized by strong heterogeneity, the volumetric flow is restricted to a smaller portion of the domain at higher flow velocities. This does not necessarily imply that the flowpaths are shallower, instead a visual inspection of the flow fields (e.g. Figure 2) suggests that the hyporheic flux is focused on highly conductive zones, which provide efficient preferential flow paths (e.g. (Fox et al., 2016; Chen and Zeng, 2015; Salehin et al., 2004; Scheibe and Yabusaki, 1998)). In homogeneous sediments  $V_{eq}$  (obtained from equation 5 and 6) does not change with conductivity but is only sensitive to changes in anisotropy. That means, anisotropic homogeneous sediments would have the same  $V_{eq}$ , as long as the ratio  $r = K_{xx}/K_{zz}$  is constant, because the hyporheic flowpaths are equally long and deep. With changes in  $r$ , flowpaths are deeper ( $r < r_0$ ) or shallower ( $r > r_0$ ) than the original ( $r_0$ ) flowpaths and thus,  $V_{eq}$  increases or decreases with  $V_{eq} \propto 1/\sqrt{r}$ .

345 Figure 3 C is color coded by the different random field methods and indicates that all methods but the Binary showed similar behavior of  $V_{eq}$ , which was also found for  $\tilde{RT}$  and  $Q_H$  (not shown here). Scenarios with the Binary random field method showed a similar trend but a lower exponential coefficient between  $\tilde{RT}$ ,  $Q_H$  and  $V_{eq}$  and  $\sigma_{\ln K}^2$ .

350 Another perspective on this data is shown in Figure 4, where  $\tilde{RT}$  is plotted over  $Q_H$  in log-log space for both heterogeneous and homogeneous realizations. We found that

$$\tilde{RT} \propto \begin{cases} Q_H^{-1} & \text{for homogeneous K of constant anisotropy r} \\ Q_H^{-2.33} & \text{for heterogeneous K} \end{cases} \quad (12)$$

i.e.  $\tilde{RT}$  tended to be significantly lower for a given  $Q_H$  under heterogeneous conditions than under isotropic homogeneous conditions, which, again, shows that a large part of the HF is restricted to a smaller part of the domain in heterogeneous sediments. On the same figure, a family of curves describing various anisotropic homogeneous scenarios is plotted. It should be noted from equation 6 that the exfiltration time and thus the median residence time  $\tilde{RT}$  depends solely on the horizontal conductivity  $K_{xx}$ , not on the vertical conductivity  $K_{zz}$  and thus not on the anisotropy of the homogeneous conductivity. This allows the design of any desired  $Q_H$  to  $\tilde{RT}$  ratio by changing either  $K_{xx}$  for changes in both  $Q_H$  and  $\tilde{RT}$  or  $K_{zz}$  for adjustments in  $Q_H$  only. Weighting the residence

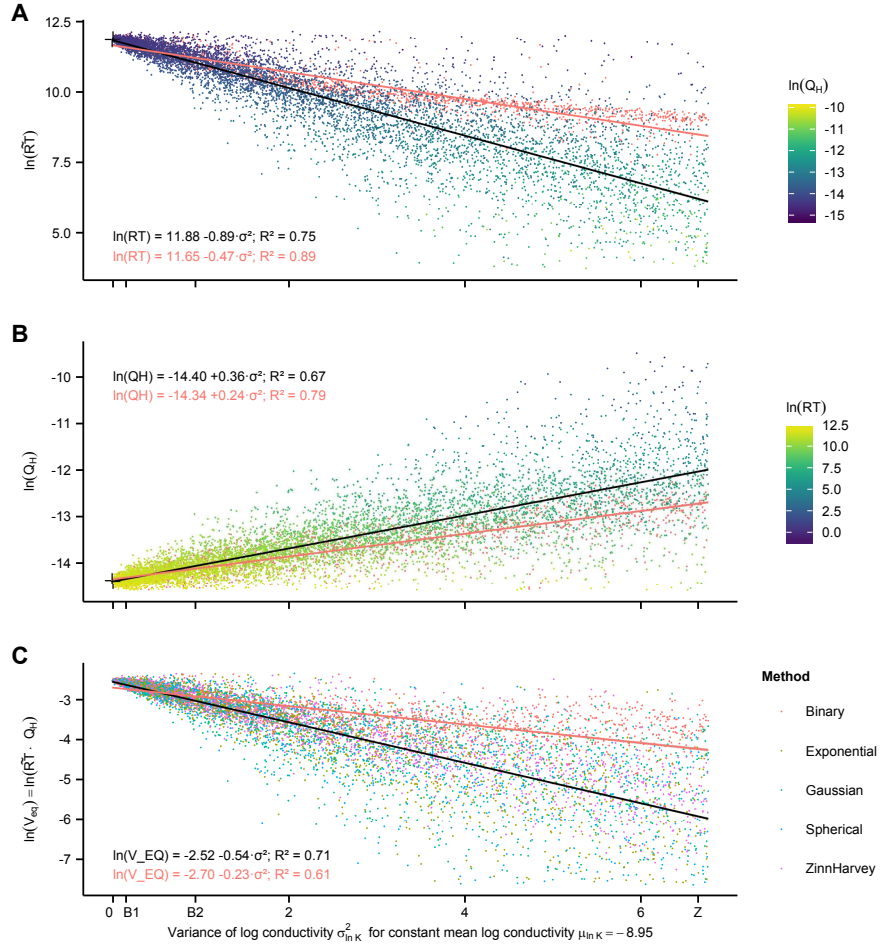


Figure 3:  $\ln(\tilde{RT})$  (**A**),  $\ln(Q_H)$  (**B**), and equivalent volume  $\ln(V_{eq})$  (**C**) for heterogeneous simulations. Each point shows the result of one simulated realization. (**A**) and (**B**) are color scaled by the respective other property to show dependencies between  $\ln(\tilde{RT})$  and  $\ln(Q_H)$  in both general trend and extreme cases. **C** is color coded by the random field method used, which highlights the similar behavior of all methods but the Binary, which is therefore color coded by method in **A** and **B** as well. In each plot, the two regressions correspond to the binary and all other methods respectively. Black crosses in **A**, **B** and **C** indicate the homogeneous case of equal  $\mu_{\ln K}$ . B1, B2 and Z on the x-axis indicate the conductivity variances used by (Sawyer and Cardenas, 2009) and (Zhou et al., 2013).

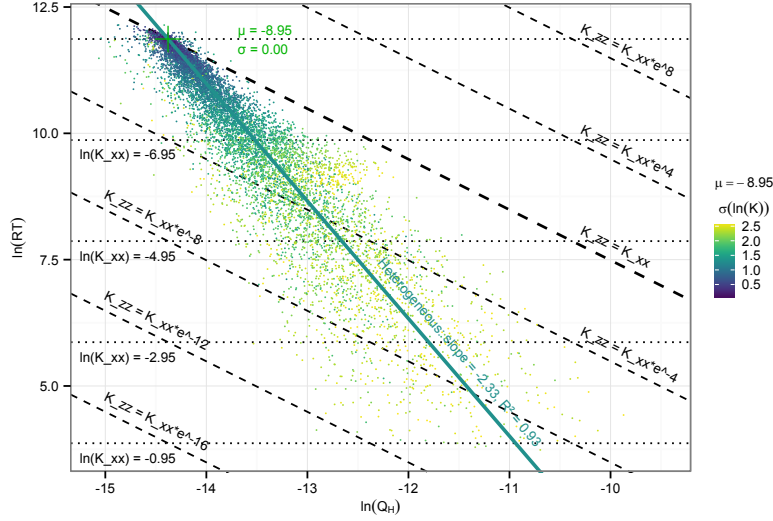


Figure 4: Heterogeneous  $Q_H$  and  $\tilde{R}T$  show an approximately inversely quadratic dependency between each other in linear space due to local concentrations of flow paths with increasing  $\sigma_{\ln K}$ . In comparison, dotted lines show  $\tilde{R}T$  of equal horizontal conductivity and dashed lines show  $\tilde{R}T$  to  $Q_H$  ratios of equal anisotropy. The bold dashed line indicates the  $\tilde{R}T$  to  $Q_H$  ratios of isotropic homogeneous cases of varying conductivity.

time by the volumetric flow of the streamtraces, as it is done in section 2.4, will  
 365 not affect this independence of the residence time of the vertical conductivity,  
 because only the magnitude of the flow is affected by  $r$  which therefore will  
 be canceled out in the weighting process. This independence of  $\tilde{R}T$  of  $K_{zz}$  is  
 shown by the horizontal dotted lines in 4, which show the  $\tilde{R}T$  to  $Q_H$  ratios for  
 homogeneous sediments of equal  $K_{xx}$  but varying  $K_{zz}$ .

370 We have tested the importance of the hydraulic conductivity of the upper  
 sediment layer, because it is known to have a strong influence on exchange  
 processes (see section 2.4). As expected from equation 9, the results of the  
 stepwise regression model suggest that both  $\tilde{R}T$  and  $Q_H$  were mainly controlled  
 by conductivity properties of the uppermost zone. To be precise, the model  
 375 selected  $\sigma_{2\% \lambda}$ ,  $\mu_{1\% \lambda}$  and  $\sigma_{5\% \lambda}$ ,  $\mu_{5\% \lambda}$  to be the two most important predictors for  
 $\tilde{R}T$  and  $Q_H$ , respectively. Further predictors, such as *random field method*,  $l_x$ ,  $l_y$   
 or  $\alpha$  had almost no relevance regarding model prediction performance (Table S3  
 & S4, supporting information). The importance of the upper layer is illustrated  
 by Figure 5, which shows the prediction performance of various models for  $\tilde{R}T$   
 380 and  $Q_H$  given the conductivity metrics  $\mu_{n, \ln K}$  and  $\sigma_{n, \ln K}$  of upper layers of  
 different thicknesses. The figure shows, that calculating  $\mu_{n, \ln K}$  and  $\sigma_{n, \ln K}$   
 from very thick layers reduces model performance by averaging the effect of  
 the important upper layer conductivity information with less important lower  
 layer information. Similarly, calculating those metrics from very thin layers  
 385 drops too much information and again decreases model performance, although

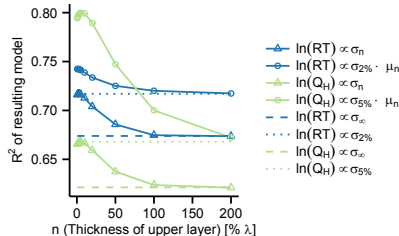


Figure 5: The coefficient of determination ( $R^2$ ) for different models (linestyles) over the thickness of the upper layer, the information of which was fed into the model. The models perform best, if the information of a thin upper layer is known. The performance decreases both, if information is averaged over a too large amount of the domain and if it is calculated from a too thin layer.

the decline in model performance was not as strong as for large layers within the boundaries of our investigations. The best prediction of  $\tilde{RT}$  and  $Q_H$  is obtained from conductivity metrics calculated from an average of 1...5% $\lambda$ , which is equivalent to 2...10 mm or 2...10 cells in this case. Finally, it has to be noted that the upper layer of a Gaussian random field is not independent of the layer underneath, which raises the need for further investigations on the importance of the upper layer of the HZ.

#### 4. Discussion

The exponential relationship between  $\tilde{RT}$ ,  $Q_H$  and  $\sigma_{\ln K}^2$  as shown in equation 10 and 11 is in good agreement with prior studies that investigated a variety of heterogeneity scenarios (figure 6). For example, Zhou et al. (2013) reported an increase of  $Q_H$  of almost one order of magnitude ( $\times 9.2$ ) in a bimodally distributed heterogeneous streambed of  $\sigma_{\ln K}^2 = 6.65$  compared to a homogeneous streambed of equal  $\mu_{\ln K}$ . Similarly, equation 11 yields an increase of  $Q_{H,Het} = 11.0Q_{H,Hom}$  and  $Q_{H,Het} = 4.9Q_{H,Hom}$  for log-normal distributed and binary distributed conductivity respectively, given the same  $\sigma_{\ln K}^2$ . In contrast to this strongly heterogeneous case, Sawyer and Cardenas (2009) and Bardini et al. (2013) assumed much lower variances of K ( $\sigma_{\ln K}^2 = 0.148$  and  $\sigma_{\ln K}^2 = 0.937$ ) for the streambeds they investigated. They argued that their streambeds were part of one depositional facies for which hydraulic conductivity tends to vary less than for sediments consisting of different depositional facies. Sawyer and Cardenas (2009) concluded that heterogeneity had a minor effect due to small changes in  $RT$  and  $Q_H$ .  $Q_H$  was found to vary only by factors of 0.8 and 1.2 compared to the homogeneous case, which is in good agreement with the factor 1.05 and 1.4 calculated from equation 11 for  $\sigma_{\ln K}^2 = 0.148$  and  $\sigma_{\ln K}^2 = 0.937$  respectively. Similarly,  $\tilde{RT}$  was found to vary by factors of 1.36 and 0.47, which is an acceptable agreement with the factor 0.88 and 0.43 calculated from equation 10. Note that Sawyer and Cardenas (2009) use an ad-

415 vanced anisotropic equivalent homogeneous case based on flux simulations rather  
 than a simple statistical equivalent like the geometric mean. This and the fact  
 that Sawyer and Cardenas (2009) simulated only one selectively placed hetero-  
 420 geneous field might explain the anomaly of the weakly heterogeneous "Massilon"  
 case. In addition to these studies, Salehin et al. (2004) investigated both  $RT$   
 and  $Q_H$  in discrete heterogeneous streambeds with  $\sigma_{\ln K}^2 = 1.0$  and  $\sigma_{\ln K}^2 = 2.0$ .  
 For  $\sigma_{\ln K}^2 = 1.0$ , Salehin et al. (2004) found  $\tilde{RT}$  to decrease in heterogeneous  
 sediments by a factor  $\approx 0.65$ , which agrees well with  $\tilde{RT}_{Het} = 0.63\tilde{RT}_{Hom}$  and  
 $\tilde{RT}_{Het} = 0.41\tilde{RT}_{Hom}$  from equation 10 for binary and log-normal distributed  
 conductivity respectively. However, the ratio between  $\tilde{RT}$  for the heterogeneous  
 and homogeneous cases was found to be almost equal ( $\approx 0.64$ ) under  $\sigma_{\ln K}^2 = 2.0$ ,  
 425 which is contradictory to our general findings but a good example of how vari-  
 able  $Q_H$  and  $\tilde{RT}$  may be for single experiments. This variability is indicated  
 by the increase in  $Q_H$ - and  $\tilde{RT}$ -variance with  $\sigma_{\ln K}^2$  in Figure 3 and emphasizes  
 that our findings are most useful for large scale or upscaling techniques, whereas  
 single small domains that do not behave ergodic may show a different behavior.  
 430 The importance of the uppermost layer, which is shown in Figure 5 and was  
 previously reported by Kalbus et al. (2009) is a possible explanation for the un-  
 expected similarity between the two heterogeneous experiments by Salehin et al.  
 (2004). In both experiments, a layer of homogeneous sand was added to the top  
 of the heterogeneous sediment to shape the bedforms. Consequently, both ex-  
 435 periments had equal hydraulic conductivity of the uppermost zone, which might  
 have overruled the effects of the different heterogeneous structures underneath.

Pryshlak et al. (2015) investigated hyporheic exchange comparing a large  
 variety of both high contrast ( $7.6 < \sigma_{\ln K}^2 < 11.9$ ) and low contrast ( $0.84 <$   
 440  $\sigma_{\ln K}^2 < 1.32$ ) binary heterogeneous sediments to homogeneous sediments of  
 equal  $\mu_{\ln K}$ . Pryshlak et al. (2015) provides a data set of 20 RTDs and HF for  
 different heterogeneous and homogeneous scenarios, which allowed the evalua-  
 tion of equation 11 and 10 on a relatively large data basis. We found the data  
 to be in good agreement with our model, given that the variance of both  $RT$   
 445 and  $Q_H$  tends to increase with variance in  $K$ . Note that the original article was  
 corrected for an erratum concerning the relevant data in April 2018.

Similar to our approach, Tonina et al. (2016) conducted Monte-Carlo simula-  
 tions of heterogeneous hyporheic sediments but their results do not agree with  
 our findings. Contrary to our findings, they predicted weakly declining  $Q_H$   
 450 and increasing median  $RT$  with  $\sigma_{\ln K}^2$ . The data basis of both our study and  
 (Tonina et al., 2016) is large enough to rule out stochastic deviations, i.e. the  
 difference of their results must be systematically based on the different study  
 design. One potential reason for the different results is the effect of gaining  
 groundwater flux, which has been included in Tonina et al. (2016). However,  
 455 Fox et al. (2016) conducted similar simulations including both gaining and los-  
 ing conditions without finding such an effect. Other than that, the domain  
 size and shape, the stream trace analysis or the random field generation might  
 play a role but we could not identify the most decisive factor for the observed

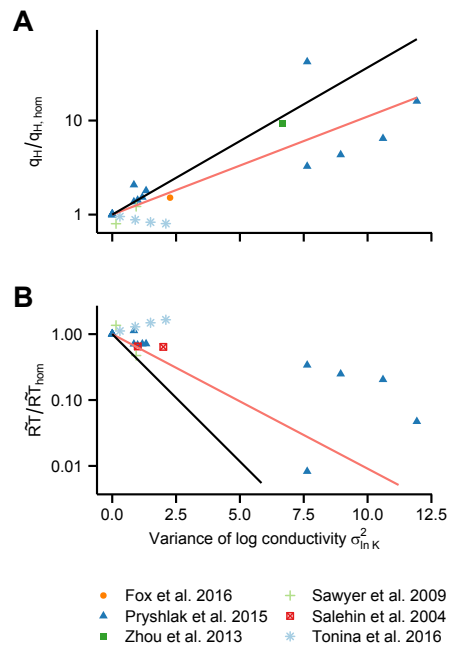


Figure 6: Relative changes in median residence time and total hyporheic flux over variance of heterogeneous conductivity. Results from literature compared to the exponential model from equation 10 and 11 for binary (pink line) and continuous (black line) heterogeneity. Similarities and differences between the study-designs and results are discussed in section 4.

discrepancies with absolute certainty.

460 Finally, Fox et al. (2016) investigated the effect of ternary-clustered heterogeneity and concluded that the isotropic homogeneous geometric mean conductivity needs to be corrected by a factor of  $e^{0.183\sigma^2}$  to match heterogeneous  $Q_H$  which is close to the factor of  $e^{0.24\sigma^2}$  for binary fields in equation 11.

465 Cardenas et al. (2004) introduced the dimensionless number  $N_H$  to quantify the influence of heterogeneity compared to external forcing mechanisms, denoted as  $N_E$ , on the geometry of the HZ.  $N_H$  was defined as

$$N_H = \frac{\sigma_{\ln K}^2 l_v}{z_{HZ}} \quad (13)$$

and  $N_E$  was defined as

$$N_E = \frac{4h_0}{\lambda s} \quad (14)$$

470 with the vertical extend of the homogeneous HZ  $z_{HZ}$  and the vertical correlation length  $l_v$ , which is calculated from  $l_x$ ,  $l_y$  and  $\alpha$  in this case.  $N_H$  was used in studies that focused on HF and hyporheic RT (e.g. (Sawyer and Cardenas, 2009; Zhou et al., 2013)), however, both Cardenas et al. (2004) and Zhou et al. (2013) emphasized the need for confirmation of its definition and significance. 475 Because of the weak influence of correlation lengths and angles on hyporheic processes found in this study, we suggest cutting the geometric variables from the dimensionless number and use

$$N_{H,new} = e^{\sigma_{\ln K}^2}, \quad (15)$$

instead of the original  $N_H$ .  $N_{H,new}$  is linearly correlated with  $\ln(\tilde{RT})$ ,  $\ln(Q_H)$  and  $\ln(V_{eq})$ . We found that  $N_{H,new}$  shows a significantly stronger correlation 480 than  $N_H$ , when used to predict any of the aforementioned HF measures. In fact, a linear regression of our data using  $N_H$  as a predictor yielded the coefficients of determination  $R_{Q_H}^2 = 0.53$ ,  $R_{\tilde{RT}}^2 = 0.49$  and  $R_{V_{eq}}^2 = 0.39$ , compared to  $R_{Q_H}^2 = 0.66$ ,  $R_{\tilde{RT}}^2 = 0.71$  and  $R_{V_{eq}}^2 = 0.64$  when using  $N_{H,new}$ .

485 Equation 12 and Figure 4 demonstrate that there is no isotropic homogeneous sediment that represents a heterogeneous sediment with respect to both  $\tilde{RT}$  and  $Q_H$ , be it based on the geometric mean, the arithmetic mean or any other isotropic conductivity. When fitting an isotropic homogeneous conductivity to match  $Q_H$ , the homogeneous  $\tilde{RT}$  will be overestimating the corresponding 490  $\tilde{RT}$  of a heterogeneous sediment and vice versa. The strength of this deviation depends on  $\sigma_{\ln K}^2$ , as shown by the color scale in Figure 4 and by  $V_{eq} = Q_H \tilde{RT}$  in Figure 3 C. For example, a homogeneous model that was fitted to match  $Q_H$  of a moderately heterogeneous sediment with  $\sigma_{\ln K}^2 = 1$  would show a  $\tilde{RT}$  that is about 1.7 times longer than the corresponding heterogeneous one. However, an 495 isotropic homogeneous model that was fitted to  $Q_H$  of a heterogeneous sediment with  $\sigma_{\ln K}^2 = 6.65$  as in (Zhou et al., 2013) would overestimate  $\tilde{RT}$  by about a factor of 36.

An equivalent homogeneous case can be obtained by choosing an anisotropic homogeneous conductivity tensor that generates equivalent results in both res-

500 idence times and hyporheic exchange. Such an equivalent anisotropic conductivity tensor can be obtained from equation 5, 6, 10 and 11:

$$\tilde{R}T_{Het} = e^{a\sigma_{\ln K}^2} \tilde{R}T_{Hom,iso} = \frac{e^{\mu_{\ln K}}}{K_{xx,eq}} \tilde{R}T_{Hom,iso} \quad (16a)$$

$$\Rightarrow K_{xx,eq} = e^{\mu_{\ln K} - a\sigma_{\ln K}^2} \quad (16b)$$

505 and

$$Q_{H,Het} = e^{b\sigma_{\ln K}^2} Q_{H,Hom,iso} = \frac{\sqrt{K_{xx,eq}K_{zz,eq}}}{e^{\mu_{\ln K}}} Q_{H,Hom,iso} \quad (17a)$$

$$\Rightarrow K_{zz,eq} = e^{\mu_{\ln K} + (2b+a)\sigma_{\ln K}^2} \quad (17b)$$

510 with  $a = -0.89, b = 0.36$  for log-normal distributed heterogeneity and  $a = -0.47, b = 0.24$  for binary distributed heterogeneity.

As an example, equations 16b and 17b can be used to calculate equivalent anisotropic conductivity vectors for the moderate and the extreme heterogeneous cases of (Sawyer and Cardenas, 2009) and (Zhou et al., 2013). The equivalent anisotropic conductivity vector for the moderate log-normal distributed heterogeneity of  $\mu_{\ln K} = -8.95$  and  $\sigma_{\ln K}^2 = 1.0$  yields  $\ln(K_{xx}) = -8.06$  and  $\ln(K_{zz}) = -9.12$  or an anisotropy ratio of  $r = 2.9$ . For the more extreme binary heterogeneity of equal  $\mu_{\ln K}$  but higher variance  $\sigma_{\ln K}^2 = 6.65$ , the equivalent anisotropic conductivity yields  $\ln(K_{xx}) = -5.82$  and  $\ln(K_{zz}) = -8.88$  or an anisotropy ratio  $r = 21.3$ . To give an additional field study based example, Pryor (1973) reported a conductivity distribution of  $\mu_{\ln K} = -7.195$  and  $\sigma_{\ln K}^2 = 0.39$  from measurements on the *Whitewater River Bar*. Assuming a lognormal conductivity distribution, we expect  $\tilde{R}T$  to decrease by 29% and  $Q_H$  to increase by 15% due to heterogeneity. The river bar could be represented by an anisotropic sediment of  $\ln(K_{xx}) = -6.85$  and  $\ln(K_{zz}) = -7.26$ , i.e an anisotropy ratio of  $r = 1.5$ .

525 It should be noted that these equivalent anisotropic homogeneous cases do not reflect the actual anisotropy of the heterogeneous fields. In fact, the independence of the heterogeneous results of correlation lengths and correlation angles indicates, that the heterogeneous fields chosen in this study have little local anisotropy at all, which is most likely due to the fact that the integral scales of the fields are of similar dimension as the hyporheic flow cells. Instead, the hyporheic flow cells of the heterogeneous and the equivalent anisotropic homogeneous cases might have completely different shape but a similar equivalent volume. The heterogeneous flow cells evolve along highly conductive areas that might be deep or shallow, whereas the anisotropic flow cells develop in shallower areas. However, this uniform reduction of flow cell depths adequately reflects the behavior of heterogeneous fields with respect to hyporheic  $\tilde{R}T$  and  $Q_H$ . This simplification is useful if the sediment is treated as an ideal reactor that is solely controlled by reaction times and concentrations, neglecting the potential need for spatial information like reaction volume or exchange depth. The fact

540

that it can be easily calculated from just the variance and median of the heterogeneous conductivity distribution makes it an ideal tool for combined field and simulation studies. As spatial information is difficult to obtain, point wise conductivity measurements could be used to calculate the required statistical metrics and improve an accompanying numerical model by using an equivalent anisotropic conductivity to simulate HF and RT.

## 5. Conclusions

Our results demonstrate that there is no unique, but yet a systematic effect of heterogeneity on hyporheic flux (HF) and residence times (RT). Thus we conclude that heterogeneity is neither generally important (Zhou et al., 2013) nor negligible (Bardini et al., 2013). The effect of heterogeneity on HF and RT depends mainly on the variance of  $K$ . In fact,  $\tilde{RT}$  decreases exponentially while  $Q_H$  increases exponentially with  $\sigma_{\ln K}^2$ . This exponential relationship can be seen in both discrete and continuous heterogeneity fields, yet exponential coefficients vary slightly between the two types.

HF is focused on smaller, high conductive, well connected fractions of the domain in heterogeneous sediments. This reduction of effective seepage volume promotes faster, focused flow and hence lower RT compared to homogeneous sediment of equal HF. As a consequence of this focusing of flow paths, there exists no equivalent isotropic homogeneous sediment that matches both HF and RT of the respective heterogeneous one. Anisotropic homogeneous sediments, however, reduce the seepage volume in a similar fashion and consequently affect HF and RT in a similar way compared to heterogeneous sediments. The anisotropic conductivity tensor presented can be used to account for the effects of heterogeneity on HF and RT without detailed knowledge of the spatial arrangement of hydrofacies and purely on the basis of statistical moments of the conductivity distribution. Both numerical and analytical models that target hyporheic exchange may benefit from this simplification, which removes the necessity to characterize the full complexity of heterogeneity and instead allows to quantify the integral impact of heterogeneity on HF and RT by means of the moments of the heterogeneity distribution.

## Appendix A. Anisotropic Hyporheic Exchange

The method shown in this section was developed by Elliott and Brooks (1997). Here, it is expanded to describe also anisotropic conductivities, which has been done in a similar fashion by (Zlotnik et al., 2011).

For a closed form solution of hyporheic exchange in an anisotropic medium, the domain of Figure 2 is simplified to a 2D semi-infinite plane. Furthermore, the head boundary condition of equation 1 is simplified to a sinusoidal head

without slope, yielding

$$580 \quad h|_{z^*=0} = h_0 \sin(x^*), \quad (\text{A.1a})$$

$$h|_{z^*=-\infty} = 0, \quad (\text{A.1b})$$

$$h|_{x^*} = h|_{x^*+2\pi} \quad (\text{A.1c})$$

585 with  $x^* = \frac{2\pi}{\lambda}x$  and  $z^* = \frac{2\pi}{\lambda}z$ . Both of these simplifications allow an easier solution of the flow field and are believed to have minor effects on the conclusions drawn from the results. On this domain, the anisotropic laplace equation

$$K_{xx} \frac{\partial^2 h}{\partial x^2} + K_{zz} \frac{\partial^2 h}{\partial z^2} = 0 \quad (\text{A.2})$$

with a diagonal conductivity tensor is solved with respect to the boundary conditions in equation A.1 by

$$590 \quad h(x, z) = h_0 e^{\sqrt{r}z^*} \sin(x^*). \quad (\text{A.3})$$

Thus, Darcy's law  $\mathbf{u} = [u_x, u_z]^T = -\mathbf{K}\nabla h$  results in the vertical and horizontal seepage velocities

$$u_x = \Phi \frac{dx}{dt} = -K_{xx} h_0 \frac{2\pi}{\lambda} e^{\sqrt{r}z^*} \cos(x^*), \quad (\text{A.4a})$$

$$595 \quad u_z = \Phi \frac{dz}{dt} = -K_{zz} h_0 \frac{2\pi}{\lambda} \sqrt{r} e^{\sqrt{r}z^*} \sin(x^*) \quad (\text{A.4b})$$

with porosity  $\Phi$  and time  $t$ . Defining  $u_0 = K_{xx} h_0 \frac{2\pi}{\lambda}$  yields

$$u_x = -u_0 e^{\sqrt{r}z^*} \cos(x^*), \quad (\text{A.5a})$$

$$u_z = -\frac{u_0}{\sqrt{r}} e^{\sqrt{r}z^*} \sin(x^*). \quad (\text{A.5b})$$

600 From this velocity field, streamtraces can be defined by the set of points with dimensionless coordinates  $X^*$  and  $Z^*$  that follow the velocity field

$$\frac{dZ^*}{dX^*} = \frac{u_z}{u_x} = \frac{1}{\sqrt{r}} \tan X^* \quad (\text{A.6})$$

and thus for a given infiltration point ( $0 \leq X_0^* < \pi/2, Z_0^* = 0, t = 0$ )

$$Z^* = -\frac{1}{\sqrt{r}} \ln \left( \frac{\cos(X^*)}{\cos(X_0^*)} \right). \quad (\text{A.7})$$

605 From A.4, A.5 and A.7 we can derive the respective  $X^*$  coordinate via

$$\Phi \frac{\lambda}{2\pi} \frac{dX^*}{dt} = -u_0 \exp\left(-\ln \left( \frac{\cos(X^*)}{\cos(X_0^*)} \right)\right) \cos(X^*) \quad (\text{A.8a})$$

$$\Rightarrow \Phi \frac{\lambda}{2\pi} \frac{dX^*}{dt} = -u_0 \cos(X_0^*) \quad (\text{A.8b})$$

$$\Rightarrow X^* = X_0^* - \frac{u_0}{\Phi} \frac{2\pi}{\lambda} t \cos(X_0^*). \quad (\text{A.8c})$$

610 For completeness, but not used here, the Z-coordinate of a streamtrace can be derived via

$$Z^* = -\frac{1}{\sqrt{r}} \ln \left( \frac{\cos(X_0^* - \frac{u_0}{\Phi} \frac{2\pi}{\lambda} t \cos(X_0^*))}{\cos(X_0^*)} \right). \quad (\text{A.9})$$

From the symmetry of the problem we know that a streamtrace that infiltrates at  $X_0^*$  exfiltrates at  $-X_0^*$ . The respective exfiltration time  $t_{RT}(X_0^*)$  can be calculated by equation A.8 as

$$t_e(X_0^*) = \frac{\Phi \lambda}{u_0 \pi} \frac{X_0^*}{\cos(X_0^*)} \quad (\text{A.10})$$

or

$$t_e(X_0) = \frac{\Phi \lambda}{K_{xx} h_0 \pi} \frac{X_0}{\cos(\frac{2\pi}{\lambda} X_0)}. \quad (\text{A.11})$$

The volumetric flow of a hyporheic streamtrace can simply be derived by its vertical seepage velocity in equation A.4 at its infiltration point

$$u_z|_{X_0, Z=0} = -h_0 \frac{2\pi}{\lambda} \frac{K_{xx}}{\sqrt{r}} \sin\left(\frac{2\pi}{\lambda} X_0\right). \quad (\text{A.12})$$

## Acknowledgments

Preprocessed simulation data and the source code that was used to generate and process the data can be found in the supporting information.

625 This research was supported by a Grant (Nr. 1158-132.8-2011) from the GIF, the German-Israeli Foundation for Scientific Research and Development. We thank Audrey Sawyer and one anonymous reviewer, whose critical and constructive comments significantly helped to improve the article.

## References

630 Ayachit, U., Avila, L.S., 2015. The ParaView guide: updated for ParaView version 4.3. Kitware Inc.

Azizian, M., Boano, F., Cook, P.L., Detwiler, R.L., Rippy, M.A., Grant, S.B., 2017. Ambient groundwater flow diminishes nitrate processing in the hyporheic zone of streams. Water Resources Research URL: <http://doi.wiley.com/10.1002/2016WR020048>, doi:10.1002/2016WR020048.

Bardini, L., Boano, F., Cardenas, M., Sawyer, A., Revelli, R., Ridolfi, L., 2013. Small-scale permeability heterogeneity has negligible effects on nutrient cycling in streambeds. Geophysical Research Letters 40, 1118–1122. URL: <http://onlinelibrary.wiley.com/store/10.1002/grl.50224/asset/grl50224.pdf?v=1&t=hety4t>, doi:10.1002/grl.50224.

- 645 Battin, T.J., Kaplan, L.A., Findlay, S., Hopkinson, C.S., Marti, E.,  
Packman, A.I., Newbold, J.D., Sabater, F., 2008. Biophysical controls on organic carbon fluxes in fluvial networks. *Nature Geoscience* 1, 95–100. URL: <http://www.nature.com/doi/finder/10.1038/ngeo101>, doi:10.1038/ngeo101.
- 650 Boano, F., Harvey, J.W., Marion, A., Packman, A.I., Revelli, R., Ridolfi, L., Wörman, A., 2014. Hyporheic flow and transport processes: Mechanisms, models, and biogeochemical implications. *Reviews of Geophysics* 52, 603–679. URL: <http://doi.wiley.com/10.1002/2012RG000417>, doi:10.1002/2012RG000417.
- 655 Boano, F., Poggi, D., Revelli, R., Ridolfi, L., 2009. Gravity-driven water exchange between streams and hyporheic zones. *Geophysical Research Letters* 36. URL: <http://doi.wiley.com/10.1029/2009GL040147>, doi:10.1029/2009GL040147.
- Cardenas, M.B., Wilson, J., 2006. Hydrodynamics of coupled flow above and below a sediment–water interface with triangular bedforms URL: <ftp://spacegrant.hawaii.edu/glazer/Chen%20References/Cardenas%202006.pdf>.
- 660 Cardenas, M.B., Wilson, J.L., Haggerty, R., 2008. Residence time of bedform-driven hyporheic exchange. *Advances in Water Resources* 31, 1382–1386. URL: <http://linkinghub.elsevier.com/retrieve/pii/S0309170808001231>, doi:10.1016/j.advwatres.2008.07.006.
- 665 Cardenas, M.B., Wilson, J.L., Zlotnik, V.A., 2004. Impact of heterogeneity, bed forms, and stream curvature on subchannel hyporheic exchange. *Water Resources Research* 40. URL: <http://doi.wiley.com/10.1029/2004WR003008>, doi:10.1029/2004WR003008.
- 670 Chen, C., Zeng, L., 2015. Using the level set method to study the effects of heterogeneity and anisotropy on hyporheic exchange: Level Set Method for Hyporheic Exchange. *Water Resources Research* 51, 3617–3634. URL: <http://doi.wiley.com/10.1002/2014WR016444>, doi:10.1002/2014WR016444.
- 675 Chen, X., 2000. Measurement of streambed hydraulic conductivity and its anisotropy. *Environmental Geology* 39, 1317–1324. URL: <http://download.springer.com/static/pdf/188/art%253A10.1007%252Fs002540000172.pdf?auth> doi:10.1007/s002540000172.
- 680 Crook, N., Binley, A., Knight, R., Robinson, D.A., Zarnetske, J., Haggerty, R., 2008. Electrical resistivity imaging of the architecture of substream sediments. *Water Resources Research* 44. URL: <http://doi.wiley.com/10.1029/2008WR006968>, doi:10.1029/2008WR006968.

- Durlafsky, L.J., 1991. Numerical calculation of equivalent grid block permeability tensors for heterogeneous porous media. *Water Resources Research* 27, 699–708. URL: <http://doi.wiley.com/10.1029/91WR00107>, doi:10.1029/91WR00107.
- 685
- Elliott, A.H., Brooks, N.H., 1997. Transfer of nonsorbing solutes to a streambed with bed forms: Theory. *Water Resources Research* 33, 123–136. doi:10.1029/96WR02784.
- Fehlman, H.M., 1985. Resistance components and velocity distributions of open channel flows over bedforms. Ph.D. thesis. Colorado State University. Fort Collins, Colorado 80523.
- 690
- Fleckenstein, J.H., Fogg, G.E., 2008. Efficient upscaling of hydraulic conductivity in heterogeneous alluvial aquifers. *Hydrogeology Journal* 16, 1239–1250. URL: <http://link.springer.com/10.1007/s10040-008-0312-3>, doi:10.1007/s10040-008-0312-3.
- 695
- Fleckenstein, J.H., Niswonger, R.G., Fogg, G.E., 2006. River-Aquifer Interactions, Geologic Heterogeneity, and Low-Flow Management. *Ground Water* 44, 837–852. URL: <http://doi.wiley.com/10.1111/j.1745-6584.2006.00190.x>, doi:10.1111/j.1745-6584.2006.00190.x.
- 700
- Fox, A., Boano, F., Arnon, S., 2014. Impact of losing and gaining streamflow conditions on hyporheic exchange fluxes induced by dune-shaped bed forms. *Water Resources Research* 50, 1895–1907. URL: <http://doi.wiley.com/10.1002/2013WR014668>, doi:10.1002/2013WR014668.
- 705
- Fox, A., Laube, G., Schmidt, C., Fleckenstein, J.H., Arnon, S., 2016. The effect of losing and gaining flow conditions on hyporheic exchange in heterogeneous streambeds. *Water Resources Research* URL: <http://doi.wiley.com/10.1002/2016WR018677>, doi:10.1002/2016WR018677.
- 710
- Gelhar, L.W., 1993. *Stochastic subsurface hydrology*. Prentice-Hall, Englewood Cliffs, N.J.
- Genereux, D.P., Leahy, S., Mitasova, H., Kennedy, C.D., Corbett, D.R., 2008. Spatial and temporal variability of streambed hydraulic conductivity in West Bear Creek, North Carolina, USA. *Journal of Hydrology* 358, 332–353. URL: <http://linkinghub.elsevier.com/retrieve/pii/S0022169408002953>, doi:10.1016/j.jhydrol.2008.06.017.
- 715
- Gomez-Velez, J.D., Krause, S., Wilson, J.L., 2014. Effect of low-permeability layers on spatial patterns of hyporheic exchange and groundwater upwelling. *Water Resources Research* 50, 5196–5215. URL: <http://doi.wiley.com/10.1002/2013WR015054>, doi:10.1002/2013WR015054.
- 720

- Gong, R., Haslauer, C.P., Chen, Y., Luo, J., 2013. Analytical relationship between Gaussian and transformed-Gaussian spatially distributed fields. *Water Resources Research* 49, 1735–1740. URL: <http://doi.wiley.com/10.1002/wrcr.20143>, doi:10.1002/wrcr.20143.
- Hester, E.T., Young, K.I., Widdowson, M.A., 2013. Mixing of surface and groundwater induced by riverbed dunes: Implications for hyporheic zone definitions and pollutant reactions. *Water Resources Research* 49, 5221–5237. URL: <http://doi.wiley.com/10.1002/wrcr.20399>, doi:10.1002/wrcr.20399.
- Irvine, D.J., Brunner, P., Franssen, H.J.H., Simmons, C.T., 2012. Heterogeneous or homogeneous? Implications of simplifying heterogeneous streambeds in models of losing streams. *Journal of Hydrology* 424–425, 16–23. URL: <http://linkinghub.elsevier.com/retrieve/pii/S0022169411008365>, doi:10.1016/j.jhydrol.2011.11.051.
- James, G., Witten, D., Hastie, T., Tibshirani, R., 2013. An Introduction to Statistical Learning. volume 103 of *Springer Texts in Statistics*. Springer New York, New York, NY. URL: <http://link.springer.com/10.1007/978-1-4614-7138-7>.
- Kalbus, E., Schmidt, C., Molson, J.W., Reinstorf, F., Schirmer, M., 2009. Influence of aquifer and streambed heterogeneity on the distribution of groundwater discharge. *Hydrology and Earth System Sciences* 13, 69–77. URL: <http://www.hydrol-earth-syst-sci.net/13/69/2009/>, doi:10.5194/hess-13-69-2009.
- Knudby, C., Carrera, J., 2005. On the relationship between indicators of geostatistical, flow and transport connectivity. *Advances in Water Resources* 28, 405–421. URL: <http://linkinghub.elsevier.com/retrieve/pii/S0309170804001599>, doi:10.1016/j.advwatres.2004.09.001.
- Liu, S., Chui, T.F.M., 2017. Impacts of Streambed Heterogeneity and Anisotropy on Residence Time of Hyporheic Zone. *Groundwater* URL: <http://doi.wiley.com/10.1111/gwat.12589>, doi:10.1111/gwat.12589.
- Lunt, I.A., Bridge, J.S., Tye, R.S., 2004. A quantitative, three-dimensional depositional model of gravelly braided rivers: Depositional model of gravel-bed rivers. *Sedimentology* 51, 377–414. URL: <http://doi.wiley.com/10.1111/j.1365-3091.2004.00627.x>, doi:10.1111/j.1365-3091.2004.00627.x.
- Mayer, K.U., Frind, E.O., Blowes, D.W., 2002. Multicomponent reactive transport modeling in variably saturated porous media using a generalized formulation for kinetically controlled reactions. *Water Resources Research* 38, 13–1–13–21. URL: <http://doi.wiley.com/10.1029/2001WR000862>, doi:10.1029/2001WR000862.

- 765 McLachlan, P., Chambers, J., Uhlemann, S., Binley, A., 2017. Geophysical characterisation of the groundwater-surface water interface. *Advances in Water Resources* 109, 302–319. URL: <http://linkinghub.elsevier.com/retrieve/pii/S0309170817304463>, doi:10.1016/j.advwatres.2017.09.016.
- 770 Morén, I., Wörman, A., Riml, J., 2017. Design of Remediation Actions for Nutrient Mitigation in the Hyporheic Zone. *Water Resources Research* 53, 8872–8899. URL: <http://doi.wiley.com/10.1002/2016WR020127>, doi:10.1002/2016WR020127.
- 775 Newcomer, M.E., Hubbard, S.S., Fleckenstein, J.H., Maier, U., Schmidt, C., Thullner, M., Ulrich, C., Flipo, N., Rubin, Y., 2018. Influence of hydrological perturbations and riverbed sediment characteristics on hyporheic zone respiration of CO<sub>2</sub> and N<sub>2</sub>. *Journal of Geophysical Research: Biogeosciences* URL: <http://doi.wiley.com/10.1002/2017JG004090>, doi:10.1002/2017JG004090.
- 780 Pryor, W.A., 1973. Permeability-Porosity Patterns and Variations in Some Holocene Sand Bodies. *AAPG Bulletin* 57. URL: <http://search.datapages.com/data/doi/10.1306/819A4252-16C5-11D7-8645000102C1865D>, doi:10.1306/819A4252-16C5-11D7-8645000102C1865D.
- 785 Pryshlak, T.T., Sawyer, A.H., Stonedahl, S.H., Soltanian, M.R., 2015. Multiscale hyporheic exchange through strongly heterogeneous sediments. *Water Resources Research* 51, 9127–9140. URL: <http://doi.wiley.com/10.1002/2015WR017293>, doi:10.1002/2015WR017293.
- Remy, N., Boucher, A., Wu, J., 2011. *Applied geostatistics with SGeMS: a user's guide*. Cambridge Univ Press, Cambridge.
- 790 Salehin, M., Packman, A.I., Paradis, M., 2004. Hyporheic exchange with heterogeneous streambeds: Laboratory experiments and modeling. *Water Resources Research* 40. doi:10.1029/2003wr002567.
- 795 Sawyer, A.H., Cardenas, M.B., 2009. Hyporheic flow and residence time distributions in heterogeneous cross-bedded sediment. *Water Resources Research* 45. doi:10.1029/2008wr007632.
- Scheibe, T., Yabusaki, S., 1998. Scaling of flow and transport behavior in heterogeneous groundwater systems. *Advances in Water Resources* 22, 223–238. URL: <http://www.sciencedirect.com/science/article/pii/S0309170898000141>.
- 800 Seitzinger, S., Harrison, J.A., Böhlke, J.K., Bouwman, A.F., Lowrance, R., Peterson, B., Tobias, C., Dreht, G.V., 2006. Denitrification across landscapes and waterscapes: a synthesis. *Ecological Applications* 16, 2064–2090. URL: [http://www.esajournals.org/doi/abs/10.1890/1051-0761\(2006\)016%5B2064:DALAWA%5D2.O.CO;2](http://www.esajournals.org/doi/abs/10.1890/1051-0761(2006)016%5B2064:DALAWA%5D2.O.CO;2), doi:10.1890/1051-0761(2006)016[2064:DALAWA]2.O.CO;2.

- 805 Stonedahl, S.H., Harvey, J.W., Packman, A.I., 2013. Interactions between hyporheic flow produced by stream meanders, bars, and dunes. *Water Resources Research* 49, 5450–5461. URL: <http://doi.wiley.com/10.1002/wrcr.20400>, doi:10.1002/wrcr.20400.
- 810 Stonedahl, S.H., Harvey, J.W., Wörman, A., Salehin, M., Packman, A.I., 2010. A multiscale model for integrating hyporheic exchange from ripples to meanders. *Water Resources Research* 46, n/a–n/a. URL: <http://doi.wiley.com/10.1029/2009WR008865>, doi:10.1029/2009WR008865.
- 815 Tonina, D., de Barros, F.P., Marzadri, A., Bellin, A., 2016. Does streambed heterogeneity matter for hyporheic residence time distribution in sandbedded streams? *Advances in Water Resources* 96, 120–126. URL: <http://linkinghub.elsevier.com/retrieve/pii/S0309170816302585>, doi:10.1016/j.advwatres.2016.07.009.
- 820 Trauth, N., Schmidt, C., Maier, U., Vieweg, M., Fleckenstein, J.H., 2013. Coupled 3-D stream flow and hyporheic flow model under varying stream and ambient groundwater flow conditions in a pool-riffle system. *Water Resources Research* 49, 5834–5850. URL: <http://doi.wiley.com/10.1002/wrcr.20442>, doi:10.1002/wrcr.20442.
- 825 Triska, F.J., Kennedy, V.C., Avanzino, R.J., Zellweger, G.W., Bencala, K.E., 1989. Retention and Transport of Nutrients in a Third-Order Stream in Northwestern California: Hyporheic Processes. *Ecology* 70, 1893–1905. URL: <http://doi.wiley.com/10.2307/1938120>, doi:10.2307/1938120.
- 830 Wörman, A., Packman, A.I., Marklund, L., Harvey, J.W., Stone, S.H., 2006. Exact three-dimensional spectral solution to surface-groundwater interactions with arbitrary surface topography. *Geophysical Research Letters* 33. URL: <http://doi.wiley.com/10.1029/2006GL025747>, doi:10.1029/2006GL025747.
- 835 Zhang, Y., Gable, C.W., Person, M., 2006. Equivalent hydraulic conductivity of an experimental stratigraphy: Implications for basin-scale flow simulations. *Water Resources Research* 42. URL: <http://doi.wiley.com/10.1029/2005WR004720>, doi:10.1029/2005WR004720.
- 840 Zheng, C., Gorelick, S.M., 2003. Analysis of Solute Transport in Flow Fields Influenced by Preferential Flowpaths at the Decimeter Scale. *Ground Water* 41, 142–155. URL: <http://doi.wiley.com/10.1111/j.1745-6584.2003.tb02578.x>, doi:10.1111/j.1745-6584.2003.tb02578.x.
- 845 Zhou, Y., Ritzi, R.W., Soltanian, M.R., Dominic, D.F., 2013. The Influence of Streambed Heterogeneity on Hyporheic Flow in Gravelly Rivers. *Groundwater* doi:10.1111/gwat.12048.

- Zinn, B., Harvey, C.F., 2003. When good statistical models of aquifer heterogeneity go bad: A comparison of flow, dispersion, and mass transfer in connected and multivariate Gaussian hydraulic conductivity fields. *Water Resources Research* 39. URL: <http://doi.wiley.com/10.1029/2001WR001146>,  
850 doi:10.1029/2001WR001146.
- Zlotnik, V.A., Cardenas, M.B., Toundykov, D., 2011. Effects of Multiscale Anisotropy on Basin and Hyporheic Groundwater Flow. *Ground Water* 49, 576–583. URL: <http://doi.wiley.com/10.1111/j.1745-6584.2010.00775.x>,  
855 doi:10.1111/j.1745-6584.2010.00775.x.